OXYGEN ISOTOPE DISTRIBUTIONS IN TYPE A CAIS FROM KABA, CV CARBONACEOUS CHONDRITE. K. Nagashima[1], A. N. Krot[1], G. R. Huss[1], and H. Yurimoto[2], [1]Hawai'i Institute of Geophysics and Planetology, University of Hawai'i at Mānoa, Honolulu, HI 96822, USA (kazu@higp hawaii.edu). [2]Department of Natural History Sciences, Hokkaido University, Hokkaido, Japan.

Introduction: Oxygen isotopic compositions of individual minerals in most Ca, Al-rich inclusions (CAIs) in CV chondrites are characterized by a spread along carbonaceous chondrite anhydrous mineral line: spinel and pyroxene being uniformly ^{16}O-enriched ($\Delta^{17}O \leq -20‰$) while anorthite and melilite being ^{16}O-depleted to varying degrees ($\Delta^{17}O > -20‰$) [1–2] with some exceptions [e.g., 3–9]. Although there is a general agreement that this spread is due to isotopic exchange between the initially ^{16}O-rich CAIs and an ^{16}O-poor external reservoir, the nature of this exchange and the origin of the ^{16}O-poor reservoir remain controversial. Gas-solid or gas-melt exchange in the solar nebula regions that experienced rapid fluctuations in O-isotope compositions [10] and exchange during fluid-assisted thermal metamorphism on the CV asteroidal body [11] are being discussed. Recently, a correlation between ^{16}O-depletion in melilite in CO CAIs and petrologic type of the host meteorite has been reported [12, 13]. There is also a correlation between petrologic type of a host meteorite and the degree of alteration resulting in replacement of melilite and anorthite by nepheline, sodalite, andradite, and hedenbergite in CO CAIs and chondrules [14–16]. Since all CV chondrites experienced fluid-assisted thermal metamorphism [e.g., 17], this process may have been responsible for some of O-isotopic variation in melilite and anorthite of the CV CAIs. According to the recent classification of the CV chondrites into petrologic subtypes based on Raman spectroscopy of organic matter, Kaba is the least metamorphosed (3.1) while Allende is one of the most metamorphosed (>3.6) CV chondrites [18]. Oxygen isotopic study of Kaba CAIs showed common presence of ^{16}O-rich melilite and significant variations of $\Delta^{17}O$ values of melilite within individual inclusions (from –25‰ to –3‰), unlike in the majority of igneous CAIs from Allende [19]. In order to investigate O-isotope distributions in melilites from Kaba CAIs, we conducted O-isotope imaging analyses of Kaba CAIs using the UH isotope microscope system – Cameca ims-1280 SIMS combined with two-dimensional ion detector SCAPS [8, 20].

Sample and Experimental Methods: Two thin sections containing compact Type A CAIs, HX3-A1 and FB-A1 from the oxidized CV chondrite Kaba were used in this study. The mineralogy and petrography of the CAIs were studied using the UH JEOL JXA-8500F field emission electron microprobe and JEOL 5900LV scanning electron microscope.

The analytical procedure for O-isotopography was similar to that described in [8]. A ~200 pA Cs^+ primary beam in aperture illumination mode was used to achieve uniform secondary ion emission from a sample area of ~60×80 μm^2. The normal incident electron gun was used to compensate for sample charging. The energy band pass was set to 50 eV and a contrast aperture of 150 μm in diameter was used to improve spatial resolution of the image. The exit slit was narrow enough to eliminate the contribution of interference ions to the isotopic images. The typical mass sequence and measurement time for acquiring secondary ion images was $^{27}Al^-$ (100s), $^{28}Si^-$ (100s), $^{16}O^-$ (20s), $^{18}O^-$ (1200s), and $^{16}O^-$ (20s) for one cycle. The measurement consisted of 4 cycles in total. The digital image processing using a moving-average with 3×3 pixels was applied to secondary ion ratio image in order to reduce the statistical error. The $^{18}O/^{16}O$ isotopographs were normalized to SMOW scale using $\delta^{18}O$ values of minerals obtained by spot analyses [19].

Results and Discussion: The CAIs measured for oxygen isotopes, HX3-A1 and FB-A1, have a melilite-rich core composed of gehlenitic melilite ($Åk_{0\ 5–10}$ and $Åk_{6–14}$ in FB-A1 and HX3-A1, respectively), spinel, fassaite and perovskite (Fig. 1). The melilite core of FB-A1 is rimmed by the layers of spinel, Ti-rich pyroxene (up to ~18 wt% TiO_2), diopside, and forsterite (Fig. 1a). The core of HX-A1 is rimmed by spinel, fassaite, and diopside (Fig. 1c). Both CAIs experienced aqueous alteration to various degrees resulting in formation of phyllosilicates, Na-bearing plagioclase, hedenbergite, andradite, ferroan olivine, and Cl-bearing Na-free silicate (wadalite?). Secondary grossular, monticellite, wollastonite, and forsterite, commonly observed in the Allende CAIs, are absent, consistent with the lower degree of thermal metamorphism experienced by Kaba.

Four regions in HX3-A1 and FB-A1 were mapped (Fig. 1). Each $\delta^{18}O$-isotopograph has ~5–10‰ (2σ) statistical uncertainty and lateral resolution of ~1 μm. The mapped core regions mainly consist of melilite with some spinel and fassaite. Two mapped regions include the rims (Figs. 1a,c). All four $\delta^{18}O$ isotopographs show spinel and fassaite grains in the core are uniformly ^{16}O-rich. The rims composed of spinel, ±Ti-rich pyroxene, fassaite, and diopside are similarly ^{16}O-

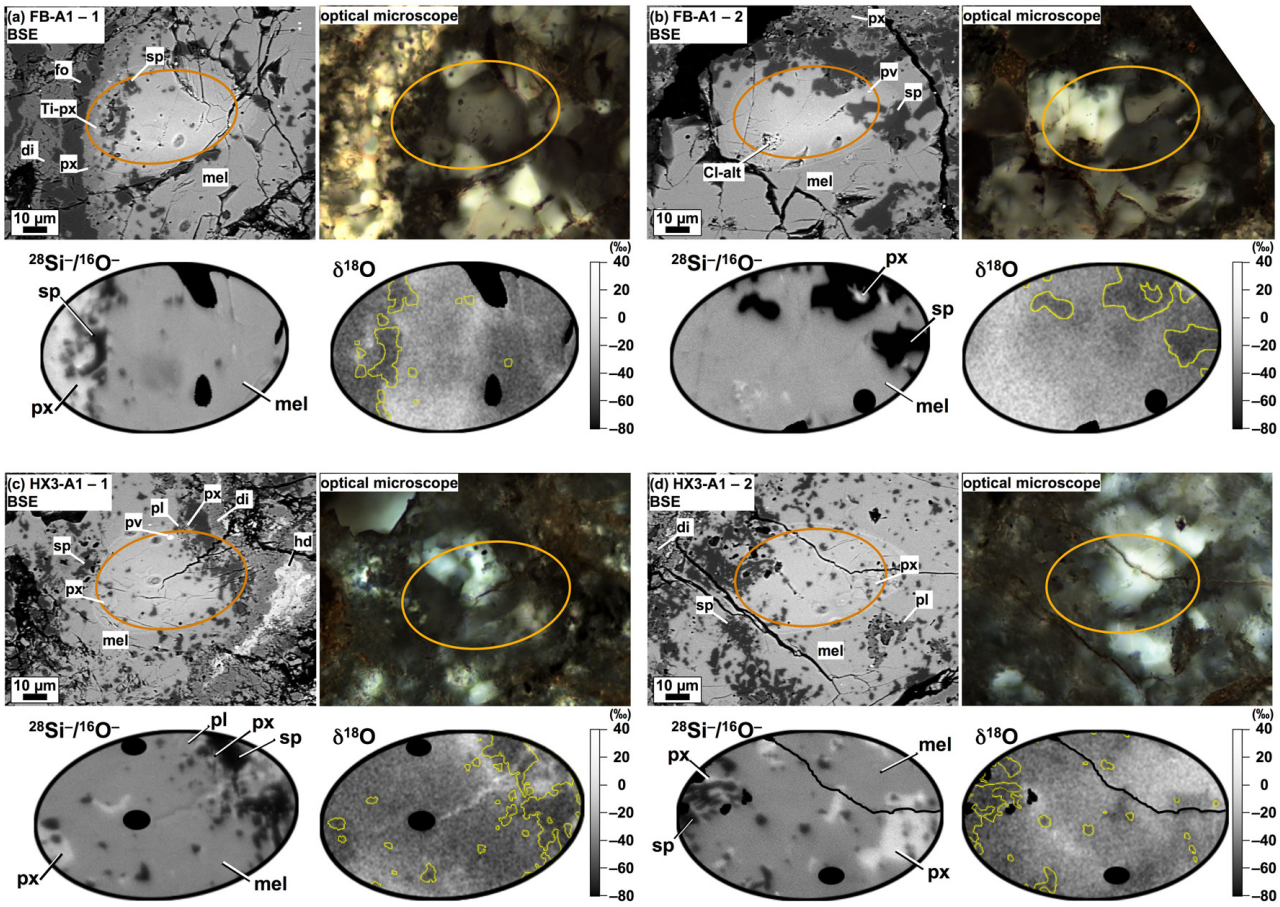

Figure 1. Backscattered-electron, optical-microscope (cross-polarized), $^{28}Si^{-}/^{16}O^{-}$, and $\delta^{18}O$ images of analyzed regions in FB-A1 (a, b) and in HX3-A1 (c,d). Regions filled by black color are masked because of artifacts due to unstable signals from cracks and holes, and due to implantation of ^{16}O primary ion beam used for previous Mg-isotope measurement. Spinel grains are outlined by yellow curves in $\delta^{18}O$ isotopographs. Cl-alt: Cl-bearing Na-free alteration phase, di: diopside, fo: forsterite, hd: hedenbergite, mel: melilite, pl: Na-bearing secondary plagioclase, px: fassaite, pv: perovskite, sp: spinel, Ti-px: Ti-rich pyroxene.

rich. Na-bearing secondary plagioclase (Fig. 1c) and Cl-bearing silicate (Fig. 1b) are ^{16}O-poor. In contrast, melilites show very complex distributions of oxygen isotopes ranging from ~–40 to +10‰ in $\delta^{18}O$. These are consistent with the results by spot analysis [19]. The $\delta^{18}O$ values change gradually within a single crystal of melilite. The sharp O-isotope boundary within single crystal reported by [3, 4, 8] is not observed in the Kaba melilites. The isotopic heterogeneities in the melilites appear to be unrelated to O-isotope compositions of the adjacent minerals. Several ^{16}O-poor regions in melilites appear to be associated with cracks and/or voids observed in backscattered-electron and optical-microscope images. These ^{16}O-poor bands are much wider than the cracks and $\delta^{18}O$ change gradually to ^{16}O-rich compositions with increasing distance from the cracks. The $\delta^{18}O$ distributions in melilites may imply O-isotopic exchange between the initially ^{16}O-rich CAIs and ^{16}O-poor external reservoir through fast O-diffusion along grain boundaries and cracks, and subsequent diffusion of ^{16}O-poor oxygen into melilite crystals.

References: [1] Clayton R. N. (1993) *Annu. Rev. Earth Planet Sci., 21,* 115–149. [2] Yurimoto H. et al. (2008) In *Reviews in Mineralogy and Geochemistry, 68,* 141–187. [3] Yurimoto H. et al. (1998) *Science, 282,* 1874–1877. [4] Ito M. et al. (2004) *GCA, 68,* 2905–2923. [5] Fagan T. J. et al. (2004) *MAPS, 39,* 1257–1272. [6] Yoshitake M. et al. (2005) *GCA, 69,* 2663–2674. [7] Aléon J. et al. (2005) *MAPS, 40,* 1043–1058. [8] Nagashima K. et al. (2010) *LPS, 41,* #2255. [9] MacPherson G. J. (2010) *MAPS, 73,* #5267. [10] Itoh S. and Yurimoto H. (2003) *Nature, 440,* 728–731. [11] Krot A. N. et al. (2008) *GCA, 72,* 2534–2555. [12] Wasson J. T. et al. (2001) *GCA, 65,* 4539–4549. [13] Itoh S. et al. (2004) *GCA, 68,* 183–194. [14] Tomeoka K. et al. (1992) *Meteoritics, 27,* 136–143. [15] Kojima T. et al. (1995) *Proc. NIPR SAM,* 8, 79. [16] Russell S. S. et al. (1998) *GCA, 62,* 689–714. [17] Krot A. N. et al. (1998) *MAPS, 33,* 1065–1085. [18] Bonal L. et al. (2006) *GCA, 70,* 1849–1863. [19] Nagashima K. et al. (2007) *LPS, 38,* #2059. [20] Nagashima K. et al. (2011) *LPS, 42,* this issue.